Nonclassical correlations between a C-band telecom photon and a stored spin-wave

Farrera, Pau; Maring, Nicolas; Albrecht, Boris; Heinze, Georg; de Riedmatten, Hugues

Published in:
Optica

DOI:
10.1364/OPTICA.3.001019

Publication date:
2016

Document version
Publisher's PDF, also known as Version of record

optica

Nonclassical correlations between a C-band telecom photon and a stored spin-wave

Pau Farrera,[1,†] Nicolas Maring,[1,†] Boris Albrecht,[1,3] Georg Heinze,[1,*] and Hugues de Riedmatten[1,2]

[1]ICFO-Institut de Ciencies Fotoniques, The Barcelona Institute of Science and Technology, 08860 Castelldefels (Barcelona), Spain
[2]ICREA-Institució Catalana de Recerca i Estudis Avançats, 08015 Barcelona, Spain
[3]Currently at Niels Bohr Institute, University of Copenhagen, København, Denmark
*Corresponding author: georg.heinze@icfo.es

Received 5 May 2016; revised 5 July 2016; accepted 2 August 2016 (Doc. ID 264586); published 9 September 2016

Future ground-based quantum information networks will likely use single photons transmitted through optical fibers to entangle individual network nodes. To extend communication distances and overcome limitations due to photon absorption in fibers, the concept of quantum repeaters has been proposed. For that purpose, it is required to achieve quantum correlations between the material nodes and photons at telecom wavelengths, which can be sent over long distances in optical fibers. Here, we demonstrate nonclassical correlation between a frequency-converted telecom C-band photon and a spin-wave stored in an atomic ensemble quantum memory. The photons emitted from the ensemble and heralding the spin-waves are converted from 780 to 1552 nm by means of an all-solid-state integrated-waveguide nonlinear device. We show ultra-low-noise operation of the device, enabling a high signal-to-noise ratio for the converted single photon, leading to a high spin-wave heralding efficiency. The presented work is an enabling step toward the practical entanglement of remote quantum memories and the entanglement of quantum systems operating at different wavelengths.

OCIS codes: (270.0270) Quantum optics; (270.5290) Photon statistics; (270.5565) Quantum communications; (130.7405) Wavelength conversion devices; (130.7408) Wavelength filtering devices; (190.4390) Nonlinear optics, integrated optics.

http://dx.doi.org/10.1364/OPTICA.3.001019

1. INTRODUCTION

Long-distance quantum communication has been an ambitious and long-standing goal in the quantum information community. Although commercial solutions are available for short-distance quantum key distribution, the extension to large scales remains challenging due to the exponential scaling of photon losses in optical fibers with distance [1]. To overcome this limitation, the concept of quantum repeaters (QR) has been developed, which holds great promise in extending the operation distance toward the continental scale [2,3].

The essential building block of most quantum repeater architectures is a photonic quantum memory (QM), which provides an interface between stationary quantum bits (encoded in atom-like systems) and flying quantum bits (encoded in photons) [4]. QMs have been implemented in many different systems, such as single atoms and ions, atomic ensembles, and various solid-state systems [3–8]. Heralded entanglement between remote QMs can be achieved by quantum interference of photonic modes correlated to the QMs at a central measurement station [9–13]. To achieve long-distance entanglement, it is essential that the heralding photon be at a telecom wavelength, in order to minimize loss in the optical fibers, which has not been the case so far in previous experiments. A crucial enabling step is therefore the ability to obtain quantum correlation between a telecom photon (preferably in the C-band, where the loss is minimal) and a long-lived atomic state in a quantum memory.

The best current QMs operate with photons in the visible or near-infrared regime [3,4], which strongly limits the possibilities of long-distance transmission. Although progress is being made toward quantum memories functioning directly at telecom wavelengths [14–16], the current demonstrations in the quantum regime still suffer from short coherence times (ns timescale) and low efficiencies. There are basically two different approaches to connect visible QMs to telecom wavelengths. The first one is to use photon pair sources intrinsically emitting entangled photon pairs with one photon at telecom wavelength and the other one in the visible or near-infrared regime to be memory compatible. This photon then can be stored in a read-write QM where the photon is mapped onto an atomic state and can be retrieved back on demand [17–24]. The second possibility is to use read QMs emitting photons entangled with the atoms and to convert the emitted photons to telecom wavelengths. Significant efforts have been devoted to quantum frequency conversion (QFC) of single photons toward the telecom band [25–34], although only very few examples involve quantum memories [26,27,32,33]. Reference [32] demonstrated the quantum frequency conversion to the C-band of a single readout photon emitted by a Rb-based quantum memory with an efficiency of

30%, using an integrated-waveguide approach. However, in that experiment there was no correlation left between the converted photon and the quantum memory. The conversion of the heralding photon from a QM was so far only realized in a single experiment in which photons were converted from 795 to 1367 nm (E-band) via four-wave mixing (FWM) in a cold and dense ensemble of rubidium atoms [26,27]. In contrast to the conversion of the readout photon, the heralding write-photon conversion is much more challenging in terms of noise suppression because the emission probability of the write photon needs to be low (typically <1%) to avoid multiple spin-wave excitations in the same mode leading to uncorrelated photons emitted in that mode. Hence, a constant background noise due to the conversion process has a much higher impact on the SNR of the heralding write photons than of the heralded read photons. In order to reach a high heralding efficiency after conversion, the background noise must therefore be very low.

In the present paper, we demonstrate low-noise quantum frequency conversion of the initial heralding write photon from a cold rubidium QM to 1552 nm via difference frequency generation in an all-solid-state integrated nonlinear waveguide. The QM is implemented in a cold ensemble of ^{87}Rb atoms following the scheme of Duan, Lukin, Cirac, and Zoller (DLCZ) [35], and we use a periodically poled lithium niobate (PPLN) waveguide for conversion. In contrast to the FWM approach in cold atoms, QFC via solid-state waveguides offers major advantages such as wavelength flexibility, robustness, relative simplicity, and excellent prospects for on-chip integration. By combining high QFC efficiency and ultra-narrowband filtering, we demonstrate that with the presented approach a high degree of nonclassical correlations between an atomic spin-wave stored in the QM and a flying telecom photon can be achieved, as well as a high signal-to-noise ratio (SNR) for the detection of the converted heralding photon, leading to a high spin-wave heralding efficiency.

2. IMPLEMENTATION AND SETUP

The experimental setup is depicted in Fig. 1(a) and basically consists of two parts: the atomic QM and the quantum frequency conversion device (QFCD). After cooling the ^{87}Rb atoms in a magneto-optical trap (MOT), they are prepared in the ground state $|g\rangle = |5^2S_{1/2}, F = 2, m_F = 2\rangle$ by optical pumping (OP) [cf. Fig. 1(b)]. A weak Gaussian-shaped write pulse (FWHM duration $\tau_W = 20$ ns), 40 MHz red-detuned from the $|g\rangle \leftrightarrow |e\rangle = |5^2P_{3/2}, F' = 2, m_F = 1\rangle$ transition, probabilistically creates a single collective spin excitation (spin-wave) between the two ground states $|g\rangle$ and $|s\rangle = |5^2S_{1/2}, F = 1, m_F = 0\rangle$. The spin-wave can be stored for a programmable time in the QM and is heralded by a Raman-scattered write photon ($\tau_w =$ 22 ns). The write photon is circularly polarized with respect to the experiments' quantization axis, set by a weak homogeneous static magnetic field applied over the whole cloud. We couple a small fraction of the isotropically emitted write photons under an angle of 3°, with respect to the write pulse axis, into a single-mode fiber (coupling efficiency approximately 60%). Besides that spatial filtering, we also perform polarization filtering of the write photon using a combination of quarter- and half-waveplates, as well as a polarization beam splitter (PBS) in front of the fiber.

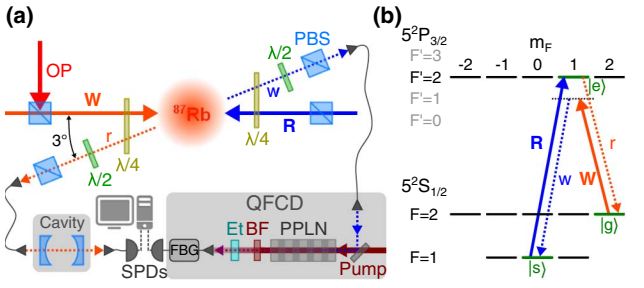

Fig. 1. (a) Experimental setup. The write pulse (W) and read pulse (R) are sent counter-propagating into the atomic cloud. Write and read photonic modes are denoted by w and r. The QFCD consists of the PPLN waveguide, a bandpass filter (BF), a narrowband etalon (Et), and a fiber Bragg grating (FBG). (b) Energy levels and coupling scheme for the DLCZ experiment.

The afterward linearly polarized write photon is sent to the QFCD and first overlapped on a dichroic mirror with the spatial mode of the pump laser at 1569 nm, which before was spectrally cleaned by two bandpass filters (Semrock NIR1, center wavelength 1570 nm, transmission bandwidth 8.9 nm), leading to a suppression of amplified spontaneous emission of more than 100 dB at 1552 nm. A combination of lenses [not shown in Fig. 1(a)] ensures optimal focusing and mode matching of the beams into the temperature-stabilized 3 cm long PPLN waveguide (HC Photonics), in which the conversion of the write photon from 780 to 1552 nm takes place. Afterward, the pump radiation is blocked by a combination of two bandpass filters (Semrock NIR01-1550/3-25), each with a transmission bandwidth of 7 nm around 1552 nm and a maximum optical depth of OD ≈ 12. However, further filtering is required to detect the converted write photon at the single-photon level because of noise generated by spontaneous Raman scattering of the pump beam, which leads to a broad background around the target wavelength. In contrast to former work [32,36], we apply additional two-stage filtering consisting of an etalon with a bandwidth of 210 MHz and a free spectral range of 4 GHz and a fiber Bragg grating (FBG) of 2.5 GHz bandwidth. The total extinction ratio of the whole filtering stage for the pump radiation at 1569 nm is >150 dB (100 dB for the two bandpass filters, 44 dB for the FBG, and 11 dB for the etalon). This allowed us to achieve high values of SNRs at a low photon number, which is necessary for the quantum frequency conversion of the heralding write single photons. The converted write photons are finally detected by an InGaAs single-photon detector (SPD) (ID Quantique ID230) with a detection efficiency of $\eta_{d,1552} = 10\%$.

3. RESULTS

A. QFCD Performance

The performance of the QFCD can be deduced from Fig. 2. For characterization of the QFCD, we couple 1.2 mW continuous wave input light at 780 nm to measure the total conversion efficiency and single-photon-level coherent input pulses of 16 ns duration with a mean photon number per pulse of $\mu_{\text{in}} =$ 0.16 to measure the SNR, both versus the coupled pump power (measured behind the waveguide). The plotted internal efficiency η_{int} excludes all optical losses, e.g., due to initial coupling in the waveguide ($\eta_{\text{cpl}} \approx 74\%$), all subsequent filtering stages ($\eta_{\text{filter}} \approx 36\%$), all optical surfaces including one optical isolator ($\eta_{\text{surf}} \approx 70\%$), and the final fiber coupling ($\eta_{\text{fiber}} \approx 75\%$). The data are fitted with the models described in [32,36], and we

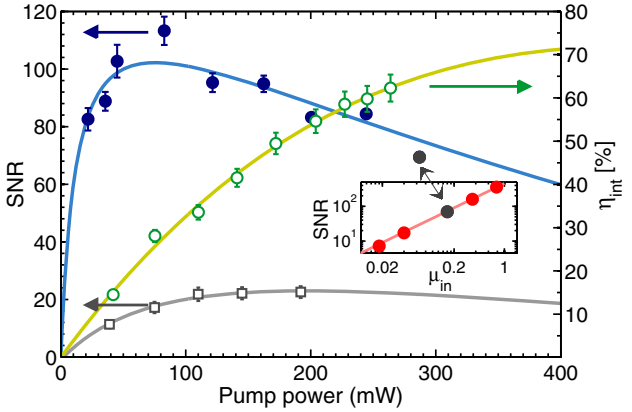

Fig. 2. Signal-to-noise ratio (SNR; left axis, blue dots for full filtering, gray squares without etalon), measured with a mean input photon number per pulse of $\mu_{in} = 0.16$, and internal efficiency η_{int} of the QFCD (right axis, green circles), measured with classical input light, versus pump power measured after the waveguide. The data are fitted by functions, modeling the expected behavior (solid lines). The inset shows the SNR versus μ_{in} for a fixed pump power of $P_{pump} = 287$ mW.

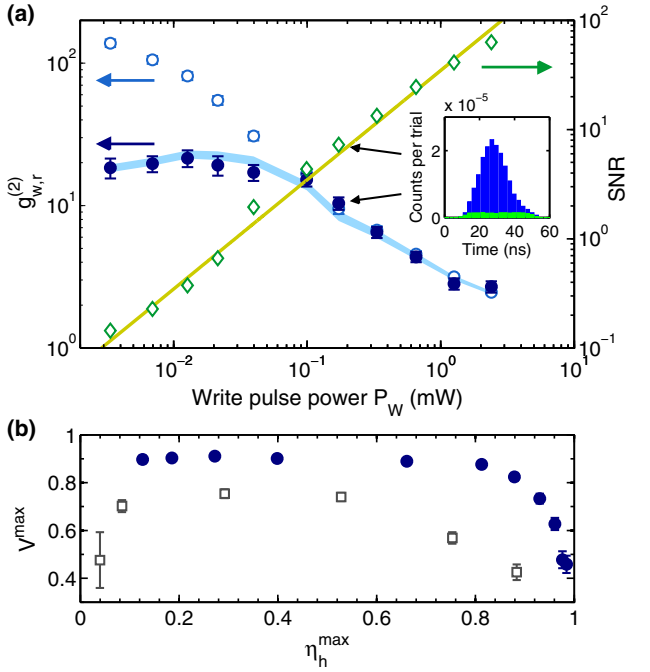

Fig. 3. (a) Normalized cross-correlation of the unconverted write photons (left axis, blue circles) and the converted ones (blue dots) with the read photons and SNR of the converted write photons (right axis, green diamonds, error bars smaller than symbol size) versus peak power of the write pulse. The blue shaded area corresponds to the expected $g^{(2)}_{cw,r}$, as inferred from Eq. (1), and the SNR is fitted with a linear regression (green line). The inset shows, as an example, the detected shape of the converted write photon for $P_W = 333$ μW. The pump power was fixed at $P_{pump} = 290$ mW. (b) Dependence of extrapolated maximal visibility V^{max} in a two atomic ensemble entanglement experiment on the maximal heralding efficiency η_h^{max} (blue dots for full filtering, gray squares without etalon).

retrieve a normalized conversion efficiency of $\eta_n = 61\%/\mathrm{W/cm^2}$ and a maximum internal efficiency of $\eta_{int}^{max} = 72\%$, which corresponds to a maximum total device efficiency of $\eta_{dev}^{max} \approx 10\%$ with $\eta_{dev} = \eta_{int}\eta_{loss}$, with $\eta_{loss} = 14\%$. The SNR, defined as the background-subtracted conversion signal over the background, follows the expected behavior (blue line), showing a drop for low pump powers due to the dark count limitation of our detector ($DC_{1552} = 10$ Hz), as well as a decrease for very high pump powers due to the nonlinear dependence of η_{int} on P_{pump}. For comparison, we also included a trace of the SNR measured without the etalon (gray squares), which shows significantly worse filtering. The inset shows the SNR dependence on the mean input photon number μ_{in} for full filtering (including the etalon) for a fixed pump power of $P_{pump} = 287$ mW. We observe the expected linear dependence $\mathrm{SNR} = \mathrm{SNR}_{max} \times \mu_{in}$ with $\mathrm{SNR}_{max} = 452$ for a single-photon input (i.e., $\mu_{in} = 1$). This represents a more than fivefold improvement compared to former reported results [32].

B. Combined QM and QFCD

Next, we combined the QFCD with the cold atomic QM to convert the write photons from 780 to 1552 nm and investigate the joint properties of the telecom photons and the atomic spin-wave stored in the QM. To create the spin-wave, weak Gaussian-shaped write pulses of $\tau_W = 20$ ns duration were sent, and the width of the write-photon detection gate was set to 40 ns [cf. green area in the inset of Fig. 3(a)]. To gain information about the spin-wave, we sent a read pulse ($\tau_R = 35$ ns, $P_R = 190$ μW) resonant to the $|s\rangle \leftrightarrow |e\rangle$ transition to convert the spin-wave back into a single read photon. Due to collective interference of the atoms, the read photon is emitted in a spatial mode given by the phase matching condition $\mathbf{k}_r = \mathbf{k}_R + \mathbf{k}_W - \mathbf{k}_w$, with $\mathbf{k}_{r,R,W,w}$ denoting the respective wave vectors of the single photons and pulses [35]. The read photon is then polarization-filtered before being sent through a monolithic Fabry–Perot cavity ($\eta_{cav} \approx 20\%$ total transmission, including cavity transmission and subsequent fiber coupling) for spectral filtering and finally detected in a window of 100 ns by a silicon SPD (Excelitas SPCM-AQRH-14) with $\eta_{d,780} = 40\%$ efficiency. The retrieval efficiency is defined as the probability to map a heralded spin-wave onto a read photon. Its raw value is calculated as $\eta_{ret} = p_{cw,r}/p_{cw}$, where $p_{cw,r}$ is the probability per trial to detect a coincidence between a converted write and a read photon, and p_{cw} is the probability per trial to obtain a detection event in the converted-write-photon detector. The fiber-coupled retrieval efficiency $\eta_{ret}^{fiber} = \eta_{ret}/(\eta_{cav}\eta_{d,780})$ corresponds to the probability of finding a read photon in the optical fiber after the vacuum cell, i.e., corrected for filtering and detector efficiency only.

To demonstrate that the conversion of the write photon preserves its quantum character, we measured the normalized second-order cross-correlation between the converted write photon and the read photon, defined as $g^{(2)}_{cw,r} = p_{cw,r}/(p_{cw}p_r)$. For comparison, we also took the cross-correlation $g^{(2)}_{w,r}$ without write-photon conversion, for which we replaced the QFCD by a Fabry–Perot filtering cavity with similar characteristics as the one used for the read photons but resonant with the write photons. The obtained data are shown in Fig. 3(a) as blue dots for $g^{(2)}_{cw,r}$ and blue circles for $g^{(2)}_{w,r}$ versus the applied power of the write pulse. We observe the highest cross-correlation of $g^{(2)}_{cw,r} \approx 20$ for a write pulse power of $P_W \approx 10$ μW. For higher P_W, $g^{(2)}_{cw,r}$ decreases, as expected for a DLCZ-type QM. For lower values of P_W, $g^{(2)}_{cw,r}$

slightly drops due to noise introduced by the QFCD and the dark counts of the SPDs [37]. This also explains the deviation of $g^{(2)}_{cw,r}$ from $g^{(2)}_{w,r}$ in the low-P_W regime. The measured $g^{(2)}_{cw,r}$ in Fig. 3(a) are well above the classical limit of 2, assuming thermal statistics for the write and read beams (see below). This shows that we can operate the combined QM-QFC device for a large range of write pulse powers in a highly nonclassical regime. The experimental data follow well the expected behavior, taking into account the background noise created by the QFCD pump laser (indicated by the blue shaded area), which can be deduced from

$$g^{(2)}_{cw,r} = \frac{g^{(2)}_{w,r} + \mathrm{SNR}^{-1}}{1 + \mathrm{SNR}^{-1}}. \quad (1)$$

Here, $g^{(2)}_{w,r}$ denotes the measured cross-correlation if the write photon is sent through a filtering cavity (similar to the read-photon cavity) instead of the QFCD, and SNR is the signal-to-noise ratio of the converted write photon. $\mathrm{SNR} = (p_{cw} - p_N)/p_N$, where p_N is the probability to have a detection when the write photon is blocked before the QFCD (see also Supplement 1). The good agreement between the experimental data and the simple model suggests that the noise generated by the QFCD pump beam is the main limiting factor for the value of $g^{(2)}_{cw,r}$.

Moreover, we proved unambiguously the high degree of nonclassical correlations between the converted write photons and the retrieved read photons by violating the Cauchy–Schwarz inequality for classical light, given by

$$R = \frac{(g^{(2)}_{cw,r})^2}{g^{(2)}_{cw,cw} \cdot g^{(2)}_{r,r}} \leq 1, \quad (2)$$

where $g^{(2)}_{cw,cw} = \frac{p_{cw,cw}}{p_{cw}p_{cw}}$ ($g^{(2)}_{r,r} = \frac{p_{r,r}}{p_r p_r}$) denotes the unheralded autocorrelation function of the converted write (read) photons. The measured correlation values for different write powers and the inferred Cauchy–Schwarz parameter R are given in Table 1. Even for relatively high write pulse powers, we clearly violate Eq. (2). For $P_W = 0.17$ mW, we obtain $R = 31$, violating the Cauchy–Schwarz inequality by more than four standard deviations and clearly demonstrating strong nonclassical correlations between the converted write photons and the retrieved read photons.

In addition to nonclassical correlations, another requirement to build a reliable QR is to achieve a high SNR in the detection of the converted heralding photon. Hence, we investigated the dependence of the SNR of the frequency-converted write photon on the write pulse power. The results are shown as green diamonds in Fig. 3(a). We observe the expected linear increase of the SNR with write pulse power as $\mathrm{SNR} \propto P_W$. For large P_W, we observe SNRs > 50 while still being in the nonclassical regime.

Table 1. Measured Values of the Coincidence Detection Probability $p_{cw,r}$, the Cross-Correlation $g^{(2)}_{cw,r}$, and the Unheralded Autocorrelations $g^{(2)}_{cw,cw}$ and $g^{(2)}_{r,r}$ of the Converted Write Photons and Read Photons for Different Write Pulse Powers P_W[a]

P_W [mW]	$p_{cw,r}$ [%]	$g^{(2)}_{cw,r}$	$g^{(2)}_{cw,cw}$	$g^{(2)}_{r,r}$	R
2.39	$4.2 \cdot 10^{-3}$	2.48(6)	2.0(2)	2.16(9)	1.4(2)
0.65	$1.2 \cdot 10^{-3}$	4.49(8)	2.3(3)	2.04(9)	4.4(7)
0.17	$0.3 \cdot 10^{-3}$	9.9(2)	1.6(4)	2.0(1)	31(7)

[a]Errors correspond to ±1 standard deviation. The Cauchy–Schwarz parameter R is calculated from Eq. (2).

From the data presented in Fig. 3(a), we can obtain more insight about the performance of our combined QM-QFC device for quantum information protocols. From the measured $g^{(2)}_{cw,r}$, we can infer the maximal visibility $V^{\max}$ that could be achieved in a two-photon interference experiment. For example, if the atomic qubit was entangled with a converted photonic qubit (e.g., in polarization [38] or time bin [39]) or in a two-ensemble entanglement experiment [40], we can infer $V^{\max} = (g^{(2)}_{cw,r} - 1)/(g^{(2)}_{cw,r} + 1)$. Here, it is assumed that the QFCD is phase-preserving [31,36]. Also, from the measured SNR, we can infer the maximal heralding efficiency $\eta_h^{\max} = \mathrm{SNR}/(\mathrm{SNR} + 1)$ of the combined QM-QFC device for heralding the presence of a spin-wave in the ensemble. The inferred $V^{\max}$ is plotted as a function of $\eta_h^{\max}$ in Fig. 3(b). We infer a visibility of $V \approx 90\%$ up to 80% heralding efficiency for full filtering (blue dots). $V^{\max}$ decreases for higher $\eta_h^{\max}$, but we still obtain $V^{\max} > 1/\sqrt{2}$, potentially enabling a violation of the Clauser–Horne–Shimony–Holt (CHSH)-type Bell inequality, for $\eta_h^{\max} > 90\%$. This confirms the suitability of the combined QM-QFC device as an elemental building block of a QR for long-distance quantum communication. If the etalon is removed, $V^{\max}$ drops significantly (cf. gray squares), clearly demonstrating the importance of ultranarrowband filtering for the all-solid-state-based QFC approach. We stress that these values are given here only to infer the potential of our device for quantum information experiments and should be confirmed with further measurements.

Finally, we investigated the capability of the combined QM-QFC device to preserve the nonclassical correlations of the converted write photons and the stored spin-wave depending on the storage time in the QM. The retrieval efficiency η_{ret} (green circles in Fig. 4) decreases over storage time due to dephasing of the stored spin-wave, which is mainly induced by thermal atomic motion and, to a smaller degree, by external spurious magnetic field gradients. The decay can be fitted with a theoretical model introduced in Supplement 1 (see green line in Fig. 4), giving a decay time of $\tau = 23.6 \pm 0.8$ μs. However, the storage time is not a fundamental limitation here, as it could be increased by orders of magnitude using other techniques [26,27,41–43]. The normalized cross-correlation $g^{(2)}_{cw,r}$ between the converted write

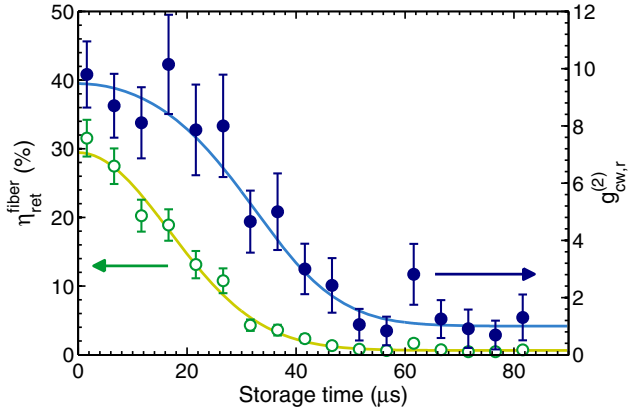

Fig. 4. Retrieval efficiency (left axis, green circles) and normalized cross-correlation of the converted write photons and read photons (right axis, blue dots) versus storage time in the QM. The write and pump powers were fixed at $P_W = 0.18$ mW and $P_{\mathrm{pump}} = 290$ mW.

photons and the retrieved read photons is shown as blue dots in Fig. 4 for a write pulse power of $P_W = 0.18$ mW. We observe the expected decay of $g^{(2)}_{cw,r}$ and fit the data with the above-mentioned model, giving a decay time of $\tau = 25.8 \pm 1.2$ μs, which is consistent with the result obtained when fitting η_{ret}. Figure 4 shows that we stay in the nonclassical regime ($g^{(2)}_{cw,r} > 2$) up to storage times of about 40 μs, which correspond to a fiber transmission length of ∼8 km.

C. Discussion

The performance of the QFCD is currently mainly limited by technical issues like coupling efficiencies in the PPLN waveguide and into the final optical fiber, as well as transmission efficiencies through the filtering stage and other optical surfaces. However, with the current device conversion efficiency of about 10% and typical fiber absorptions of 0.2 dB/km for 1552 nm and 3.5 dB/km for 780 nm, the unconverted photon traveling in a 780 nm fiber would experience a higher loss after around 3 km than a frequency-converted photon traveling in a telecom fiber. Hence, even with this seemingly low conversion efficiency, QFC beats direct transmission already after a few kilometers.

Second, we note that a QFCD converting photons to the telecom C-band with a given device efficiency η_{dev} is equivalent in terms of loss to an additional fiber length of $L = -10/0.2 \cdot \log(\eta_{\mathrm{dev}})$. For the current device efficiency of 10%, this corresponds to an additional loss of −10 dB, meaning an equivalent of 50 km extra fiber in each arm of a telecom quantum repeater. A device efficiency of 50% would correspond to 15 km of additional fiber in each arm.

Finally, we note that to alleviate the requirements for spectral filtering and thus to increase the QFC device efficiency, different conversion strategies with further separated wavelengths also could be considered [44]. A larger wavelength separation would decrease the Raman noise or could even suppress it completely. However, to convert the 780 nm photon into the telecom C-band (1530–1565 nm), where the losses in optical fibers are the lowest, not much flexibility is possible. Raman noise in PPLN is present up to 700 cm^{-1} (21 THz) away from the excitation pump, as measured in [45]. In our case, the frequency separation between the pump at 1569 nm and the target wavelength at 1552 nm is 2.1 THz. Using a pump at the edge of the gain spectrum of erbium amplifiers, around 1605 nm, the separation in frequency between that pump and the target wavelength at 1517 nm would be 11 THz, which is still inside the Raman noise window. The solution for a noise-free conversion, as mentioned in Ref. [44], would indeed be to use a pump at around 2000 nm, converting the 780 nm photons to 1280 nm—into the telecom O-band (frequency difference of 84 THz). This is an interesting approach, but one would have to deal with other issues, such as higher transmission losses in the fibers, more challenging mode matching in the nonlinear waveguide, and the need for more sophisticated technical resources.

4. CONCLUSION

In conclusion, we demonstrated highly nonclassical correlations between a frequency-converted telecom C-band photon and a spin-wave stored in an atomic quantum memory. The photon heralding the spin-wave was converted from 780 to 1552 nm using an integrated nonlinear waveguide. We showed that by improved optical filtering, very high signal-to-noise ratios, up to $\mathrm{SNR}_{\mathrm{max}} = 452$ for a weak coherent input pulse with an average of one photon per pulse, could be achieved. This was the key to obtain high nonclassical correlations between the converted write and read photons up to $g^{(2)}_{w,r} \approx 20$ when the QFCD was combined with the QM, as well as high SNRs for the detection of the converted write photon, leading to high spin-wave heralding efficiencies. Moreover, we proved that the quantum character of the converted write photons and read photons is preserved by violating the Cauchy–Schwarz inequality by more than four standard deviations. Finally, we demonstrated that the nonclassical correlations between the heralding telecom write photon and the near-infrared read photon could be stored in the QM up to 40 μs. Our experiment showed that quantum frequency conversion based on an integrated nonlinear waveguide is a viable approach to create quantum correlation between telecom photons and long-lived spin-waves. This approach offers significant advantages in terms of wavelength flexibility, robustness, and simplicity compared to frequency-conversion processes in cold atomic gases. The robust all-solid-state quantum frequency conversion of the heralding write photons in combination with the preservation and storage of nonclassical correlations in a DLCZ-QM is an important step toward the interconnection of matter nodes operating at different wavelengths and the realistic implementation of an elementary telecom quantum repeater link.

Note added in proof—After submission of our paper we learned about a related experiment [46].

Funding. European Research Council (ERC) (QuLIMA); Ministerio de Economía y Competitividad (MINECO); Fondo Europeo de Desarrollo Regional (FEDER) (FIS2012-37569); MINECO Severo Ochoa (SEV-2015-0522); AGAUR 2014 (SGR 1554); Fundació Privada Cellex.

Acknowledgment. We thank Xavier Fernandez-Gonzalvo and Matteo Cristiani for helpful discussions and support during the initial setup of the experiment. P.F. acknowledges the International PhD-fellowship program "la Caixa"-Severo Ochoa @ ICFO. G.H. acknowledges support by the ICFOnest+ international postdoctoral fellowship program.

[†]These authors contributed equally to this work.

See Supplement 1 for supporting content.

REFERENCES

1. B. Korzh, C. C. W. Lim, R. Houlmann, N. Gisin, M. J. Li, D. Nolan, B. Sanguinetti, R. Thew, and H. Zbinden, "Provably secure and practical quantum key distribution over 307 km of optical fibre," Nat. Photonics **9**, 163–168 (2015).
2. H.-J. Briegel, W. Dür, J. I. Cirac, and P. Zoller, "Quantum repeaters: the role of imperfect local operations in quantum communication," Phys. Rev. Lett. **81**, 5932–5935 (1998).
3. N. Sangouard, C. Simon, H. de Riedmatten, and N. Gisin, "Quantum repeaters based on atomic ensembles and linear optics," Rev. Mod. Phys. **83**, 33–80 (2011).
4. M. Afzelius, N. Gisin, and H. de Riedmatten, "Quantum memory for photons," Phys. Today **68**(12), 42–47 (2015).
5. A. I. Lvovsky, B. C. Sanders, and W. Tittel, "Optical quantum memory," Nat. Photonics **3**, 706–714 (2009).

6. K. Hammerer, A. S. Sørensen, and E. S. Polzik, "Quantum interface between light and atomic ensembles," Rev. Mod. Phys. **82**, 1041–1093 (2010).
7. C. Simon, M. Afzelius, J. Appel, A. Boyer de la Giroday, S. J. Dewhurst, N. Gisin, C. Y. Hu, F. Jelezko, S. Kröll, J. H. Müller, J. Nunn, E. S. Polzik, J. G. Rarity, H. De Riedmatten, W. Rosenfeld, A. J. Shields, N. Sköld, R. M. Stevenson, R. Thew, I. A. Walmsley, M. C. Weber, H. Weinfurter, J. Wrachtrup, and R. J. Young, "Quantum memories," Eur. Phys. J. D **58**, 1–22 (2010).
8. F. Bussières, N. Sangouard, M. Afzelius, H. de Riedmatten, C. Simon, and W. Tittel, "Prospective applications of optical quantum memories," J. Mod. Opt. **60**, 1519–1537 (2013).
9. C. W. Chou, H. de Riedmatten, D. Felinto, S. V. Polyakov, S. J. van Enk, and H. J. Kimble, "Measurement-induced entanglement for excitation stored in remote atomic ensembles," Nature **438**, 828–832 (2005).
10. C.-W. Chou, J. Laurat, H. Deng, K. S. Choi, H. de Riedmatten, D. Felinto, and H. J. Kimble, "Functional quantum nodes for entanglement distribution over scalable quantum networks," Science **316**, 1316–1320 (2007).
11. Z.-S. Yuan, Y.-A. Chen, B. Zhao, S. Chen, J. Schmiedmayer, and J.-W. Pan, "Experimental demonstration of a BDCZ quantum repeater node," Nature **454**, 1098–1101 (2008).
12. D. L. Moehring, P. Maunz, S. Olmschenk, K. C. Younge, D. N. Matsukevich, L.-M. Duan, and C. Monroe, "Entanglement of single-atom quantum bits at a distance," Nature **449**, 68–71 (2007).
13. B. Hensen, H. Bernien, A. E. Dréau, A. Reiserer, N. Kalb, M. S. Blok, J. Ruitenberg, R. F. L. Vermeulen, R. N. Schouten, C. Abellán, W. Amaya, V. Pruneri, M. W. Mitchell, M. Markham, D. J. Twitchen, D. Elkouss, S. Wehner, T. H. Taminiau, and R. Hanson, "Loophole-free Bell inequality violation using electron spins separated by 1.3 kilometres," Nature **526**, 682–686 (2015).
14. B. Lauritzen, J. Minář, H. de Riedmatten, M. Afzelius, N. Sangouard, C. Simon, and N. Gisin, "Telecommunication-wavelength solid-state memory at the single photon level," Phys. Rev. Lett. **104**, 080502 (2010).
15. J. Dajczgewand, J.-L. Le Gouët, A. Louchet-Chauvet, and T. Chanelière, "Large efficiency at telecom wavelength for optical quantum memories," Opt. Lett. **39**, 2711–2714 (2014).
16. E. Saglamyurek, J. Jin, V. B. Verma, M. D. Shaw, F. Marsili, S. W. Nam, D. Oblak, and W. Tittel, "Quantum storage of entangled telecom-wavelength photons in an erbium-doped optical fibre," Nat. Photonics **9**, 83–87 (2015).
17. C. Simon, H. de Riedmatten, M. Afzelius, N. Sangouard, H. Zbinden, and N. Gisin, "Quantum repeaters with photon pair sources and multimode memories," Phys. Rev. Lett. **98**, 190503 (2007).
18. C. Clausen, I. Usmani, F. Bussières, N. Sangouard, M. Afzelius, H. de Riedmatten, and N. Gisin, "Quantum storage of photonic entanglement in a crystal," Nature **469**, 508–511 (2011).
19. E. Saglamyurek, N. Sinclair, J. Jin, J. A. Slater, D. Oblak, F. Bussières, M. George, R. Ricken, W. Sohler, and W. Tittel, "Broadband waveguide quantum memory for entangled photons," Nature **469**, 512–515 (2011).
20. D. Rieländer, K. Kutluer, P. M. Ledingham, M. Gündoğan, J. Fekete, M. Mazzera, and H. de Riedmatten, "Quantum storage of heralded single photons in a praseodymium-doped crystal," Phys. Rev. Lett. **112**, 040504 (2014).
21. F. Bussières, C. Clausen, A. Tiranov, B. Korzh, V. B. Verma, S. W. Nam, F. Marsili, A. Ferrier, P. Goldner, H. Herrmann, C. Silberhorn, W. Sohler, M. Afzelius, and N. Gisin, "Quantum teleportation from a telecom-wavelength photon to a solid-state quantum memory," Nat. Photonics **8**, 775–778 (2014).
22. A. Lenhard, M. Bock, C. Becher, S. Kucera, J. Brito, P. Eich, P. Müller, and J. Eschner, "Telecom-heralded single-photon absorption by a single atom," Phys. Rev. A **92**, 063827 (2015).
23. G. Schunk, U. Vogl, D. V. Strekalov, M. Förtsch, F. Sedlmeir, H. G. L. Schwefel, M. Göbelt, S. Christiansen, G. Leuchs, and C. Marquardt, "Interfacing transitions of different alkali atoms and telecom bands using one narrowband photon pair source," Optica **2**, 773–778 (2015).
24. W. Zhang, D.-S. Ding, S. Shi, Y. Li, Z.-Y. Zhou, B.-S. Shi, and G.-C. Guo, "Storing a single photon as a spin wave entangled with a flying photon in the telecommunication bandwidth," Phys. Rev. A **93**, 022316 (2016).
25. S. Tanzilli, W. Tittel, M. Halder, O. Alibart, P. Baldi, N. Gisin, and H. Zbinden, "A photonic quantum information interface," Nature **437**, 116–120 (2005).
26. A. G. Radnaev, Y. O. Dudin, R. Zhao, H. H. Jen, S. D. Jenkins, A. Kuzmich, and T. A. B. Kennedy, "A quantum memory with telecom-wavelength conversion," Nat. Phys. **6**, 894–899 (2010).
27. Y. O. Dudin, A. G. Radnaev, R. Zhao, J. Z. Blumoff, T. A. B. Kennedy, and A. Kuzmich, "Entanglement of light-shift compensated atomic spin waves with telecom light," Phys. Rev. Lett. **105**, 260502 (2010).
28. R. Ikuta, Y. Kusaka, T. Kitano, H. Kato, T. Yamamoto, M. Koashi, and N. Imoto, "Wide-band quantum interface for visible-to-telecommunication wavelength conversion," Nat. Commun. **2**, 1544 (2011).
29. S. Zaske, A. Lenhard, C. A. Keßler, J. Kettler, C. Hepp, C. Arend, R. Albrecht, W.-M. Schulz, M. Jetter, P. Michler, and C. Becher, "Visible-to-telecom quantum frequency conversion of light from a single quantum emitter," Phys. Rev. Lett. **109**, 147404 (2012).
30. S. Ates, I. Agha, A. Gulinatti, I. Rech, M. T. Rakher, A. Badolato, and K. Srinivasan, "Two-photon interference using background-free quantum frequency conversion of single photons emitted by an InAs quantum dot," Phys. Rev. Lett. **109**, 147405 (2012).
31. R. Ikuta, H. Kato, Y. Kusaka, S. Miki, T. Yamashita, H. Terai, M. Fujiwara, T. Yamamoto, M. Koashi, M. Sasaki, Z. Wang, and N. Imoto, "High-fidelity conversion of photonic quantum information to telecommunication wavelength with superconducting single-photon detectors," Phys. Rev. A **87**, 010301 (2013).
32. B. Albrecht, P. Farrera, X. Fernandez-Gonzalvo, M. Cristiani, and H. de Riedmatten, "A waveguide frequency converter connecting rubidium-based quantum memories to the telecom C-band," Nat. Commun. **5**, 3376 (2014).
33. N. Maring, K. Kutluer, J. Cohen, M. Cristiani, M. Mazzera, P. M. Ledingham, and H. de Riedmatten, "Storage of up-converted telecom photons in a doped crystal," New J. Phys. **16**, 113021 (2014).
34. F. Kaiser, A. Issautier, L. A. Ngah, D. Aktas, T. Delord, and S. Tanzilli, "Toward continuous-wave regime teleportation for light matter quantum relay stations," IEEE J. Sel. Top. Quantum Electron. **21**, 69–77 (2015).
35. L. M. Duan, M. D. Lukin, J. I. Cirac, and P. Zoller, "Long-distance quantum communication with atomic ensembles and linear optics," Nature **414**, 413–418 (2001).
36. X. Fernandez-Gonzalvo, G. Corrielli, B. Albrecht, M. Grimau, M. Cristiani, and H. de Riedmatten, "Quantum frequency conversion of quantum memory compatible photons to telecommunication wavelengths," Opt. Express **21**, 19473–19487 (2013).
37. P. Sekatski, N. Sangouard, F. Bussières, C. Clausen, N. Gisin, and H. Zbinden, "Detector imperfections in photon-pair source characterization," J. Phys. B **45**, 124016 (2012).
38. H. de Riedmatten, J. Laurat, C. W. Chou, E. W. Schomburg, D. Felinto, and H. J. Kimble, "Direct measurement of decoherence for entanglement between a photon and stored atomic excitation," Phys. Rev. Lett. **97**, 113603 (2006).
39. B. Albrecht, P. Farrera, G. Heinze, M. Cristiani, and H. de Riedmatten, "Controlled rephasing of single collective spin excitations in a cold atomic quantum memory," Phys. Rev. Lett. **115**, 160501 (2015).
40. J. Laurat, K. S. Choi, H. Deng, C. W. Chou, and H. J. Kimble, "Heralded entanglement between atomic ensembles: preparation, decoherence, and scaling," Phys. Rev. Lett. **99**, 180504 (2007).
41. X.-H. Bao, A. Reingruber, P. Dietrich, J. Rui, A. Dück, T. Strassel, L. Li, N.-L. Liu, B. Zhao, and J.-W. Pan, "Efficient and long-lived quantum memory with cold atoms inside a ring cavity," Nat. Phys. **8**, 517–521 (2012).
42. S.-J. Yang, X.-J. Wang, X.-H. Bao, and J.-W. Pan, "An efficient quantum light-matter interface with sub-second lifetime," Nat. Photonics **10**, 381–384 (2016).
43. Y. Jiang, J. Rui, X.-H. Bao, and J.-W. Pan, "Dynamical zeroing of spin-wave momentum to suppress motional dephasing in an atomic-ensemble quantum memory," Phys. Rev. A **93**, 063819 (2016).
44. J. S. Pelc, L. Yu, K. De Greve, P. L. McMahon, C. M. Natarajan, V. Esfandyarpour, S. Maier, C. Schneider, M. Kamp, S. Höfling, R. H. Hadfield, A. Forchel, Y. Yamamoto, and M. M. Fejer, "Downconversion quantum interface for a single quantum dot spin and 1550-nm single-photon channel," Opt. Express **20**, 27510–27519 (2012).
45. S. Zaske, A. Lenhard, and C. Becher, "Efficient frequency downconversion at the single photon level from the red spectral range to the telecommunications C-band," Opt. Express **19**, 12825–12836 (2011).
46. R. Ikuta, T. Kobayashi, K. Matsuki, S. Miki, T. Yamashita, H. Terai, T. Yamamoto, M. Koashi, T. Mukai, and N. Imoto, "Heralded single excitation of atomic ensemble via solid-state-based telecom photon detection," arXiv:1607.01465